

Numerical Investigation of Triaxially Strained Graphene Under a Homogeneous Magnetic Field

Rohit Dilip

April 21, 2019

As the first strictly two-dimensional material ever discovered, graphene provides a veritable playground of new physics, from the fractional quantum Hall effect (FQHE) ([8], [13]) to magic angle superconductivity ([2]). Because electrons in graphene behave like massless Dirac fermions, graphene functions as a bridge between quantum field theory and condensed matter. In terms of technological applications, graphene's high Young's modulus (≈ 1.0 TPa) and intrinsic strength (130 GPa) suggest uses in construction and mechanical engineering, and strips of graphene have been demonstrated to function as effective transistors ([9]).

Evidently, characterizing the physical properties of graphene is of interest to the scientific community. In particular, the electronic applications and appearance of FQHE states in graphene suggest that understanding graphene's behavior under a magnetic field would be particularly useful. When a magnetic field is applied to a graphene flake, the density of states formed discretized levels called Landau levels.

A similar effect occurs under the application of a strain field ([4]). For a given amount of strain, one can define a pseudomagnetic field that behaves similarly to a standard magnetic field (with a defined vector potential) with two caveats. First, unlike a real magnetic field, a pseudomagnetic field does not violate time-reversal symmetry. Secondly, a real magnetic field exhibits gauge invariance, where the particular vector potential chosen is only unique up to the addition of the gradient of a function ($\mathbf{A} \rightarrow \mathbf{A} + \nabla f$ without changing the dynamics of the system). This invariance does not exist in the case of a pseudomagnetic field. The Hamiltonian that describes the dynamics of a particle in strained graphene ([10]) contains a term $v_0 \sigma_i A_i$, where v_0 is the Fermi velocity of an electron on the lattice, σ_i is a Pauli matrix, and A_i is a component of the vector potential. The addition of a function ∇f to the vector potential would result in a nontrivial term in the Hamiltonian.

Large magnetic fields are often physically difficult to realize (the National High Magnetic Field Laboratory in Florida has a maximum output of 36 T); in contrast, applying a precise strain is significantly easier to achieve. Pseudomagnetic fields are thus particularly salient to experimental groups. The physical distinctions between real and pseudomagnetic fields open the question of how the pseudomagnetic field interacts with a real magnetic field, which is the subject of this work.

This work is divided into four additional sections. In the first section, we provide a brief overview of the relevant physical properties of graphene, with references to additional literature as necessary. In the second section, we use numerical simulations to demonstrate that the interaction between a real magnetic field B and a small pseudomagnetic field B_S , rather than being qualitatively equivalent to a field $B + B_S$, actually splits the Landau levels (a phenomenon undocumented in any existing literature). In the third section, we use a variety of perturbative methods to demonstrate that the most recent models for strained graphene (which were developed using symmetry approaches in [6]) fail to extract this splitting. In the final section, we discuss potential avenues to develop more sophisticated Hamiltonians that describe strain physics.

1 Physical structure of graphene

This section provides a brief overview of the crystallographic structure of graphene. This review is non-exhaustive; a more thorough description is presented in [3]. Graphene possesses a hexagonal structure, and is composed entirely of carbon atoms. The interactions between adjacent sites are due to the overlap of the $|2s\rangle$, $|2p_x\rangle$, and $|2p_y\rangle$ orbitals. These interactions lead to sp^2 hybridization, and the new hybrid orbitals are linear combinations of the s and p_i orbitals.

The hexagonal structure of graphene is described using a two-atom basis for a triangular Bravais lattice. The lattice vectors and nearest neighbor (NN) vectors are

$$\begin{aligned} \mathbf{a}_1 &= \sqrt{3}a\mathbf{e}_x & \mathbf{a}_2 &= \frac{\sqrt{3}}{2}a(\mathbf{e}_x + \sqrt{3}\mathbf{e}_y) \\ \boldsymbol{\delta}_1 &= \frac{a}{2}(\sqrt{3}\mathbf{e}_x + \mathbf{e}_y) & \boldsymbol{\delta}_2 &= \frac{a}{2}(-\sqrt{3}\mathbf{e}_x + \mathbf{e}_y) & \boldsymbol{\delta}_3 &= -a\mathbf{e}_y \end{aligned} \quad (1)$$

where $a \approx 0.142$ nm is the nearest neighbor distance. This is explicitly shown in Figure 1.

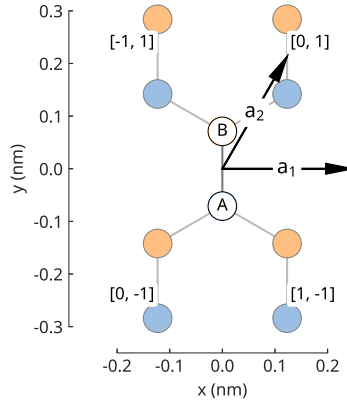


Figure 1: The physical structure of graphene. The lattice is decorated with a two-atom basis, labelled as A and B in this figure. The lattice vectors \mathbf{a}_i translate along the same sublattice, while the nearest neighbor vectors $\boldsymbol{\delta}_i$ move between sublattices.

2 Simulational Results

The simplest way to simulate the dynamics of a crystal is using the tight-binding method. The explicit formalism of the tight-binding method is well documented (for instance, see [12] or [1]) and will not be discussed here. In a tight binding model, a hopping energy t is associated with each bond between nearest neighbors (one can also associate a term for next-nearest neighbors, which are on the same sublattice). The tight-binding method can be used to analytically find energies for unstrained graphene (see [4]).

To implement a magnetic field, one uses the Peierl's substitution, which adds an additional phase associated with the magnetic field. The exact description of the Peierl's phase is given by

$$t \rightarrow t \exp \left\{ \frac{e}{\hbar} \int_{\mathbf{r}_n}^{\mathbf{r}_{n+1}} \mathbf{A} \cdot \mathbf{r} d\mathbf{r} \right\} \quad (2)$$

In this expression, \mathbf{A} is the chosen vector potential for the magnetic field¹. This is an excellent approximation in the regime where $a \ll \sqrt{\frac{\hbar}{eB}}$.

Strain effects should carry an additional adjustment to the tight-binding parameter. In this work, we primarily focus on triaxial strain, which can be roughly visualized as pulling along three planar axes (see Figure 2).

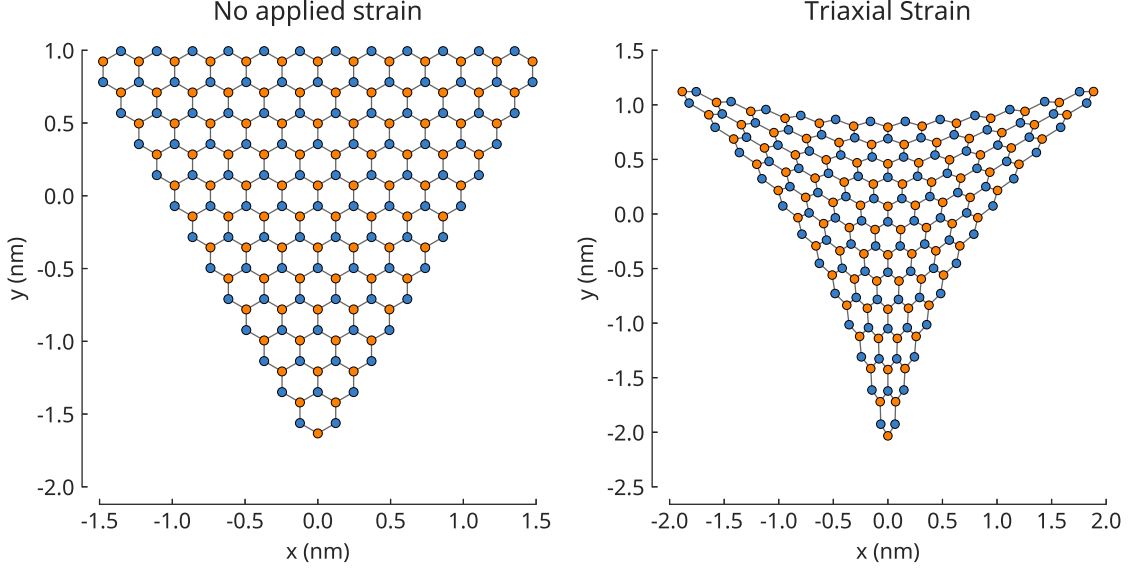


Figure 2: (Left) An unstrained lattice. (Right) A strain field corresponding to 10000 T (for visualization purposes).

The modification due to strain for the hopping across two particular sites is given by ([7])

$$t \rightarrow t \exp\{-\beta(d_n/a - 1)\} \quad (3)$$

In this expression, $\beta = -\frac{\partial \ln t}{\partial \ln a} \approx 3.37$, $a \approx 0.142$ nm is the usual NN distance, and d_n is the length of the bond between the sites under consideration. Clearly in the zero strain case there is no change in the hopping energy.

In principle, it is easy to now construct a tight binding Hamiltonian and diagonalize it, then plot the eigenenergy distribution to examine the density of states. In practice, this is somewhat difficult. The resolution at which Landau levels are clearly visible and not washed out by graphene's large Van Hove singularities requires a graphene lattice on the order of 30 nm by 30 nm³. The memory required to diagonalize matrices of this size is prohibitively large, which presents a significant barrier to further computational investigations.

¹Some care must be taken when using this expression with periodic boundary conditions. The vector potential in general is not periodic (for instance, $\mathbf{A} = (0, Bx, 0)$). The transition from one side of the lattice to the other must be chosen to carry an unphysical phase of $\exp\{2\pi i n\}$, with n an integer.

²The RHS of the inequality is known as the magnetic length.

³This is simply to see Landau levels. To witness nontrivial effects such as splittings and shifts, one would want even larger matrices

2.1 The Kernel Polynomial Method

To surmount computational barriers, we utilized the Kernel Polynomial Method (KPM) to directly compute the density of states. The KPM relies on the observation that a function $f : [-1, 1] \rightarrow \mathbb{R}$ can be expanded in terms of orthonormal Chebyshev polynomials as

$$f(x) = \sum_{n=0}^{\infty} \frac{\langle f|T_n\rangle_1}{\langle T_n|T_n\rangle_1} T_n(x) = \alpha_0 + 2 \sum_{n=1}^{\infty} \alpha_n T_n(x) \quad (4)$$

where the coefficients $\alpha_n = \langle f|T_n\rangle_1 = \int_{-1}^1 \frac{f(x)T_n(x)}{\pi\sqrt{1-x^2}} dx$. The weighting function $1/\sqrt{1-x^2}$ generally makes the integration computationally expensive, but some rearrangement gives

$$f(x) = \frac{1}{\sqrt{1-x^2}} \left[\mu_0 + 2 \sum_{n=1}^{\infty} \mu_n T_n(x) \right] \quad (5)$$

$$\mu_n = \int_{-1}^1 f(x) T_n(x) dx$$

Using Equation 5 and rescaling the Hamiltonian so the eigenvalues lie in the interval $[-1, 1]$ (this can be done by directly calculating the extremal eigenvalues of the Hamiltonian using the Lanczos algorithm ([5])), one can directly calculate the μ_n , which are known as moments. There are two classes of moments. The first take the form of expectation values over Chebyshev polynomials

$$\mu_n = \langle \beta | T_n(\tilde{H}) | \alpha \rangle \quad (6)$$

where \tilde{H} is the rescaled Hamiltonian. The states $|\alpha_n\rangle = T_n(\tilde{H}) |\alpha\rangle$ can be constructed by using the standard recursion relations associated with Chebyshev polynomials. Explicitly,

$$\begin{aligned} |\alpha_0\rangle &= |\alpha\rangle \\ |\alpha_1\rangle &= \tilde{H} |\alpha_0\rangle \\ |\alpha_{k+1}\rangle &= 2\tilde{H} |\alpha_k\rangle - |\alpha_{k-1}\rangle \end{aligned} \quad (7)$$

These moments can thus be easily calculated. For sparse matrices with dimension D , the total computational complexity to calculate N moments is $O(ND)$.

The second class of moments involve a trace over the entire Hilbert space. Explicitly evaluating these moments would be computationally taxing. Instead, one can stochastically evaluate the moments using a small subset of random vectors. For instance, these moments often take the form $\mu_n = \text{Tr}[AT_n(\tilde{H})]$. This can be written as

$$\mu_n = \text{Tr}[AT_n(\tilde{H})] \approx \frac{1}{R} \sum_{r=0}^{R-1} \langle r | AT_n(\tilde{H}) | r \rangle \quad (8)$$

We can now explicitly apply this formalism to the density of states $\rho(E)$, which is given by

$$\rho(E) = \sum_{k=0}^{D-1} \delta(E - E_k) = \text{Tr}[\delta(E - H)] \quad (9)$$

To find the density of states, we set $A = I$, and thus

$$\rho(E) = \text{Tr}[\delta(E - H)] \approx \frac{1}{R} \sum_r \langle r | \delta(E - H) | r \rangle \quad (10)$$

The accuracy of the KPM can be tuned further by expanding the number of random vectors or the order to which the Chebyshev expansion is carried out. There are a number of further computational considerations – for instance, dampening Gibbs oscillations – that arise in implementations of the KPM. For more details, see [11] for a thorough discussion.

2.2 Landau Level Splitting

Using the Peierl’s phase and the strain factor to set of a tight binding Hamiltonian, then using the Kernel Polynomial Method to extract the density of states enables one to clearly see the effect of the strain field on the Landau levels. The Landau levels asymmetrically split, as shown in Figure 3.

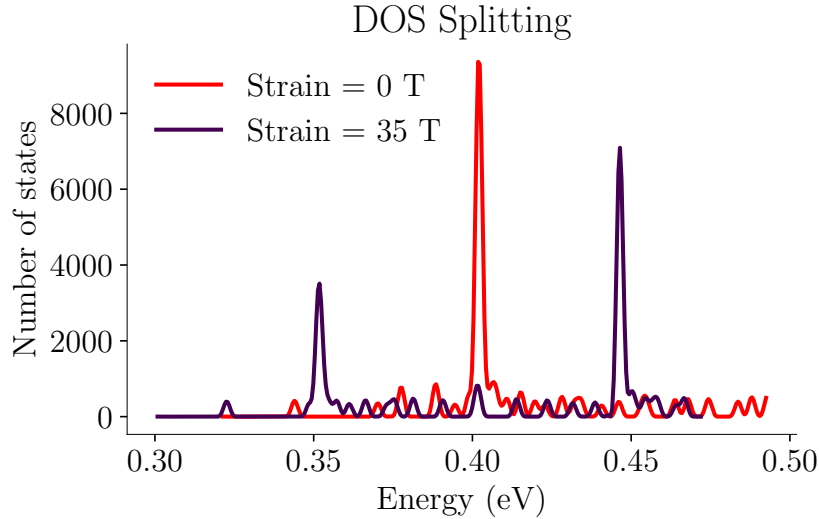


Figure 3: This plot displays asymmetric splitting of the density of states as a result of a small strain field. The strain field is labelled in terms of the equivalent pseudomagnetic field, which can be analytically determined.

Far away from $E = 0$, the splitting becomes harder to see. This is a natural product of the KPM procedure, which works well for the eigenvalues smallest in magnitude. Nonetheless, this asymmetric pattern consistently holds for 7-8 Landau levels. This splitting is a feature undocumented in existing literature, and represents an exciting deviation from existing predictions surrounding the pseudomagnetic field.

Finally, note that the splitting width scales linearly with the strain field strength, as shown in Figure ??.

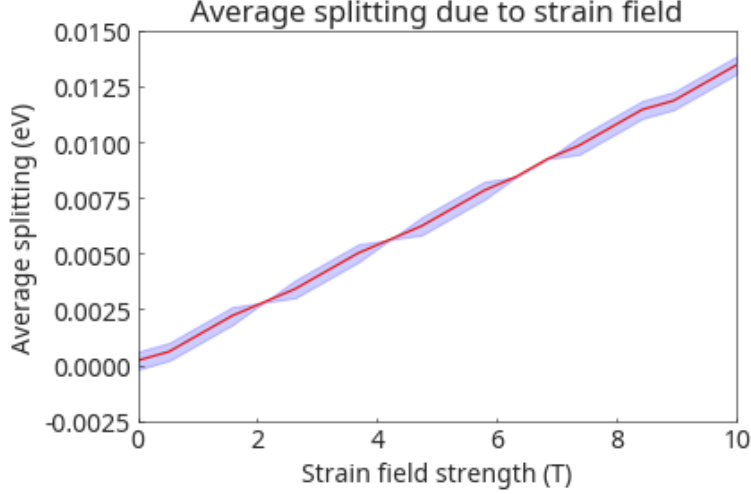


Figure 4: The average splitting width plotted against the applied strain field. The error bars (shaded) are calculated from the asymmetry between the peaks.

3 Analytic Results

In this section, I use strain Hamiltonians derived in [6] in an attempt to recover the features discovered via simulation.

3.1 Expressing all quantities in terms of ladder operators

First, I diagonalize the Hamiltonian for graphene in a magnetic field using two sets of ladder operators. I make the following definitions.

$$\pi_i = p_i - A_i^S \quad b = \frac{1}{\sqrt{2B}}(\pi_x + i\pi_y) \quad a = b^\dagger - i\sqrt{\frac{B}{2}}\bar{z} \quad (11)$$

A^R is the vector potential for a magnetic field of strength B . I will choose the symmetric gauge defined by $A^R = \frac{B}{2}(y, -x)$. Each pair of operators b, b^\dagger and a, a^\dagger satisfy the canonical commutation relations; moreover, $[b, a^\dagger] = [b, a] = 0$. b, b^\dagger move between Landau levels, and a, a^\dagger move between degenerate states within a given Landau level. $z = x + iy$, and $\bar{z} = x - iy$.

I can now write

$$\begin{aligned} \pi_x &= \sqrt{\frac{B}{2}}(b + b^\dagger) & \pi_y &= \sqrt{\frac{B}{2}}\frac{1}{i}(b - b^\dagger) \\ x &= \frac{i}{\sqrt{2B}}(a - a^\dagger + b - b^\dagger) & y &= \frac{1}{\sqrt{2B}}(b + b^\dagger - a - a^\dagger) \end{aligned} \quad (12)$$

3.2 Strained Hamiltonian

The Hamiltonian for strained graphene in the continuum limit, from [10], is

$$H = iv_{ij}(x)\sigma_i\partial_j + iv_0\sigma_i\Gamma_i - v_0\sigma_iA_i \quad (13)$$

where $v_{ij}(x)$ is the tensorial Fermi velocity (that arises due to the strain), v_0 is the Fermi velocity of graphene given by $3a_0t/2$ (a_0 is the nearest neighbor distance, t is the hopping energy associated with nearest neighbor hops in the tight-binding approximation), A_i is the vector potential associated with the pseudomagnetic field arising from the strain (this is distinct from the A_i^R in Equation 11, which describes the real magnetic field), σ_i are the Pauli matrices, and Γ_i is a vector field defined by $\Gamma_i = \frac{1}{2v_0}\partial_j v_{ij}$. Before writing these quantities explicitly, I pick the applied strain field to be triaxial strain (which creates a uniform pseudomagnetic field). Triaxial strain is described by the transformation

$$x \rightarrow x + 2cxy \quad y \rightarrow y + c(x^2 - y^2) \quad (14)$$

c is a parameter that tunes the strength of the applied pseudomagnetic field. The two dimensional strain tensor $u_{ij} = (1/2)(\partial_j u_i + \partial_i u_j + (\partial_i z)(\partial_j z))$, where u_i is the displacement in the i axis, is given by

$$\begin{aligned} u_{xx} &= 2cy & u_{xy} &= 2cx \\ u_{yx} &= 2cx & u_{yy} &= -2cy \end{aligned} \quad (15)$$

I now explicitly write all the quantities in Equation 13. Γ_i and $v_{ij}(x)$ account for both the strain and the shift in the lattice sites.

$$\begin{aligned} A_x &= -\frac{\beta}{2a_0}(u_{xx} - u_{yy}) = -\frac{2\beta c}{a_0}y & A_y &= -\frac{\beta}{2a_0}(-2u_{xy}) = \frac{2\beta c}{a_0}x \\ v_{ij}(x) &= v_0[\delta_{ij} - \frac{\beta}{4}(2u_{ij} + \delta_{ij}u_{kk}) + \tilde{u}_{ij}] \\ &= v_0[\delta_{ij} + (1 - \frac{\beta}{2})u_{ij}] \end{aligned} \quad (16)$$

\tilde{u}_{ij} is the linearized component of the strain tensor. Since there is no vertical change, $\tilde{u}_{ij} = u_{ij}$. Moreover, the strain tensor is traceless, so $u_{kk} = 0$. The vector field $\Gamma_i = \frac{1}{2v_0}\partial_j v_{ij}$ is 0, as shown below. A_i has an additional negative sign relative to [10]. Physically, this ensures that $\nabla \times \mathbf{A}$ is in the $+\hat{z}$ direction.

$$\begin{aligned} \Gamma_x &= \partial_x v_{xx} + \partial_y v_{xy} = \frac{1 - \beta/2}{2}(0 + 0) = 0 \\ \Gamma_y &= \partial_y v_{yy} + \partial_x v_{yx} = \frac{1 - \beta/2}{2}(-2c + 2c) = 0 \end{aligned} \quad (17)$$

I apply the Peierl's substitution to account for the application of a real magnetic field, so the final Hamiltonian is

$$H = -v_{ij}(x)\sigma_i\pi_j - v_0\sigma_i A_i \quad (18)$$

The Hamiltonian describing graphene under a real magnetic field is given by $H = -v_0\sigma_i\pi_i$. Working in the basis of eigenstates of this Hamiltonian, the perturbation Hamiltonian can be written as

$$H' = -v'_{ij}(x)\sigma_i\pi_j - v_0\sigma_i A_i \quad (19)$$

where $v'_{ij}(x) = v_0(1 - \frac{\beta}{2})u_{ij}$.

3.3 Expansion of H'

My strategy now will be to expand H' in terms of ladder operators $a, a^\dagger, b, b^\dagger$.

$$\begin{aligned}
 H' &= -v'_{ij}\sigma_i\pi_j - v_0\sigma_iA_i \\
 &= -\left\{ \left[(1 - \beta/2)y\pi_x + (1 - \beta/2)x\pi_y \right] \sigma_x + \left[(1 - \beta/2)x\pi_x - (1 - \beta/2)y\pi_y \right] \sigma_y \right\} \\
 &\quad - \frac{2\beta cv_0}{a_0} (-y\sigma_x + x\sigma_y)
 \end{aligned} \tag{20}$$

Factoring out the Pauli matrices and grouping terms yields

$$\begin{aligned}
 \sigma_x \text{ terms: } & (\beta/2 - 1)y\pi_x + (\beta/2 - 1)x\pi_y + \frac{2v_0\beta c}{a_0}y \\
 \sigma_y \text{ terms: } & (\beta/2 - 1)x\pi_x - (\beta/2 - 1)y\pi_y - \frac{2v_0\beta c}{a_0}x
 \end{aligned} \tag{21}$$

Inserting the ladder operator expressions into the σ_x terms gives

$$\begin{aligned}
 & (\beta/2 - 1) \left\{ \frac{(b + b^\dagger - a - a^\dagger)}{\sqrt{2B}} \sqrt{\frac{B}{2}}(b + b^\dagger) \right\} + (\beta/2 - 1) \left\{ \frac{(b^\dagger - b - a + a^\dagger)}{i\sqrt{2B}} \sqrt{\frac{B}{2}}i(b^\dagger - b) \right\} \\
 & \quad + \frac{2v_0\beta c}{a_0} \left(\frac{(b + b^\dagger) - (a + a^\dagger)}{\sqrt{2B}} \right) \\
 & = (\beta/2 - 1) \left(\frac{1}{2} \right) (b^2 + b^\dagger b - ab - a^\dagger b + bb^\dagger + (b^\dagger)^2 - ab^\dagger - a^\dagger b^\dagger) \\
 & \quad + (\beta/2 - 1) \left(\frac{1}{2} \right) ((b^\dagger)^2 - bb^\dagger - ab^\dagger + a^\dagger b^\dagger - b^\dagger b + b^2 + ab - a^\dagger b) \\
 & \quad + \frac{2v_0\beta c}{a_0} \left(\frac{(b + b^\dagger) - (a + a^\dagger)}{\sqrt{2B}} \right) \\
 & = (\beta/2 - 1)(b^2 - a^\dagger b + (b^\dagger)^2 - ab^\dagger) + \sqrt{\frac{2}{B}} \frac{v_0\beta c}{a_0} (b + b^\dagger - a - a^\dagger)
 \end{aligned} \tag{22}$$

Similarly, the σ_y terms give

$$\begin{aligned}
& (\beta/2 - 1) \left\{ \frac{(b^\dagger - b - a + a^\dagger)}{i\sqrt{2B}} \sqrt{\frac{B}{2}}(b + b^\dagger) \right\} \\
& - (\beta/2 - 1) \left\{ \frac{(b + b^\dagger - a - a^\dagger)}{\sqrt{2B}} \sqrt{\frac{B}{2}} i(b^\dagger - b) \right\} \\
& \quad - \frac{2v_0\beta c}{a_0} \left(\frac{b^\dagger - b - a + a^\dagger}{i\sqrt{2B}} \right) \\
& = (\beta/2 - 1) \left(\frac{1}{2} \right) (-i) (b^\dagger b - b^2 - ab + a^\dagger b + (b^\dagger)^2 - bb^\dagger - ab^\dagger + a^\dagger b^\dagger) \\
& \quad + (\beta/2 - 1) \left(\frac{1}{2} \right) (-i) (bb^\dagger + (b^\dagger)^2 - ab^\dagger - a^\dagger b^\dagger - b^2 - b^\dagger b + ab + a^\dagger b) \\
& \quad \quad - \sqrt{\frac{2}{B}} \frac{v_0\beta c}{ia_0} (b^\dagger - b - a + a^\dagger) \\
& = (\beta/2 - 1) (-i) (-b^2 + a^\dagger b + (b^\dagger)^2 - ab^\dagger) - \sqrt{\frac{2}{B}} \frac{v_0\beta c}{ia_0} (b^\dagger - b - a + a^\dagger)
\end{aligned} \tag{23}$$

Because the eigenvalues of the magnetic field Hamiltonian $H = -v_0\sigma_i\pi_i$ take the form $\begin{pmatrix} |n, m\rangle \\ |n-1, m\rangle \end{pmatrix}$, the only terms that lead to nonzero matrix elements in the Hamiltonian within the degenerate subspace are those that have the form $\begin{pmatrix} 0 & f \\ g & 0 \end{pmatrix}$, where f has one more b^\dagger than b , and g has one more b than b^\dagger . Throwing away terms that do not match these conditions, and using Equations 22 and 23 and the explicit form of the Pauli matrices gives

$$\begin{aligned}
f & = \left[(\beta/2 - 1)(-a) + \sqrt{\frac{2}{B}} \frac{v_0\beta c}{a_0} - (\beta/2 - 1)(-a) + \sqrt{\frac{2}{B}} \frac{v_0\beta c}{a_0} \right] b^\dagger \\
g & = \left[(\beta/2 - 1)(-a^\dagger) + \sqrt{\frac{2}{B}} \frac{v_0\beta c}{a_0} + (\beta/2 - 1)(a^\dagger) + \sqrt{\frac{2}{B}} \frac{v_0\beta c}{a_0} \right] b \\
& \Rightarrow \sqrt{\frac{2}{B}} \frac{2v_0\beta c}{a_0} \begin{pmatrix} 0 & b^\dagger \\ b & 0 \end{pmatrix}
\end{aligned} \tag{24}$$

This takes exactly the same form as the magnetic field Hamiltonian. The first order correction to the magnetic field energy levels will be

$$\begin{aligned}
& \sqrt{\frac{2}{B}} \frac{2v_0\beta c}{a_0} (\langle n, m' | \langle n-1, m' |) \begin{pmatrix} 0 & b^\dagger \\ b & 0 \end{pmatrix} \begin{pmatrix} |n, m\rangle \\ |n-1, m\rangle \end{pmatrix} \\
& = \frac{4\sqrt{2}v_0\beta c}{\sqrt{B}a_0} \sqrt{n}\delta_{mm'}
\end{aligned} \tag{25}$$

3.4 σ_z Term

The first order treatment thus fails to break the perturbation, which is at odds with our observation that the simulated splitting scales linearly with the applied strain field. However, [6] introduces an additional term proportional to σ_z , the structure of which suggests it may be successful in splitting the Landau levels.

The generalized Hamiltonian presented in [6] has seven terms H_i , i ranges from 0 to 6. $H_1, H_3, H_4 = 0$ (H_3 is negligible due to the appearance of a NNN term). Notably, we have already done the work to find most of this Hamiltonian in terms of ladder operators, since $\sum_{i=0}^5 H_i$ is precisely the Hamiltonian we had written previously. To treat this Hamiltonian perturbatively, one would make the Peierl's substitution and consider the shift from $\sum_{i=1}^6 H_i$.

First, we evaluate H_6 . I work in units where $\beta = -\frac{\partial \log t}{\partial \log a}$ is positive.

$$H_6 = [\partial_y(u_{xx} - u_{yy}) + 2\partial_x u_{xy}] \sigma_x = 8c\sigma_x \quad (26)$$

As usual, c refers to the tuning parameter we use to describe the triaxial strain, not to the speed of light. Again, we consider only nonzero matrix elements of the Hamiltonian within a degenerate subspace described by the quantum number m . The Hamiltonian now takes the form

$$H' = \begin{pmatrix} 3cV'a^2 & f \\ g & -3cV'a^2 \end{pmatrix} \quad (27)$$

I have added the requisite constant a_6 . Once again, for $(\langle n, m | \langle n-1, m | H' \begin{pmatrix} |n, m\rangle \\ |n-1, m\rangle \end{pmatrix}$, the nonzero terms of f have one more b^\dagger than b , and vice versa for g . This is the same condition we originally imposed, so the only change is now the first order correction is

$$\begin{aligned} & \sqrt{\frac{2}{B}} \frac{2v_0\beta c}{a_0} (\langle n, m' | \langle n-1, m' |) \begin{pmatrix} 3cV'a^2 & b^\dagger \\ b & -3cV'a^2 \end{pmatrix} \begin{pmatrix} |n, m\rangle \\ |n-1, m\rangle \end{pmatrix} \\ &= \sqrt{\frac{2}{B}} \frac{2v_0\beta c}{a_0} (\langle n, m' | \langle n-1, m' |) \begin{pmatrix} (3cV'a^2 + \sqrt{n}) |n, m\rangle \\ (-3cV'a^2 + \sqrt{n}) |n-1, m\rangle \end{pmatrix} \\ &= \sqrt{\frac{2}{B}} \frac{2v_0\beta c}{a_0} [(3cV'a^2 + \sqrt{n}) \delta_{mm'} + (-3cV'a^2 + \sqrt{n}) \delta_{mm'}] \\ &= \sqrt{\frac{2}{B}} \frac{4v_0\beta c}{a_0} \sqrt{n} \delta_{mm'} \end{aligned} \quad (28)$$

which is precisely the result we arrived at earlier. First order perturbation theory does not seem to reveal the split in the degeneracy.

4 Outlook and Conclusion

Our computational work predicts that a strain field will split the Landau levels, and will do so to first order in perturbation theory. This is in tension with the existing Hamiltonians that describe strained graphene. In particular, a symmetry based analysis of the Hamiltonian used in this work ([6]) suggests that this Hamiltonian captures all the relevant terms in the small- k expansion. This suggests that strain effects might become relevant far from the Dirac points in graphene. This would indicate that the continuum limit, which goes to first order in k -space, is not an accurate descriptor of strain effects. To date, it is believed that most of the interesting physical properties are captured by the continuum limit; if the second order expansion captures these effects, it would reflect a significant new development in the physics of graphene.

References

- [1] Neil W Ashcroft and N David Mermin. Solid state physics (saunders college, philadelphia, 1976). *Appendix N*, 2010.
- [2] Yuan Cao, Valla Fatemi, Shiang Fang, Kenji Watanabe, Takashi Taniguchi, Efthimios Kaxiras, and Pablo Jarillo-Herrero. Unconventional superconductivity in magic-angle graphene superlattices. *Nature*, 556(7699):43, 2018.
- [3] Jean-Noel Fuchs and Mark Oliver Goerbig. Introduction to the physical properties of graphene. *Lecture notes*, 2008.
- [4] MO Goerbig. Electronic properties of graphene in a strong magnetic field. *Reviews of Modern Physics*, 83(4):1193, 2011.
- [5] Cornelius Lanczos. *An iteration method for the solution of the eigenvalue problem of linear differential and integral operators*. United States Governm. Press Office Los Angeles, CA, 1950.
- [6] Juan L Manes, Fernando de Juan, Mauricio Sturla, and Maria AH Vozmediano. Generalized effective hamiltonian for graphene under nonuniform strain. *Physical Review B*, 88(15):155405, 2013.
- [7] M Ramezani Masir, D Moldovan, and FM Peeters. Pseudo magnetic field in strained graphene: Revisited. *Solid State Communications*, 175:76–82, 2013.
- [8] Kostya S Novoselov, Andre K Geim, SVb Morozov, Da Jiang, MIc Katsnelson, IVa Grigorieva, SVb Dubonos, Firsov, and AA. Two-dimensional gas of massless dirac fermions in graphene. *nature*, 438(7065):197, 2005.
- [9] LA Ponomarenko, F Schedin, MI Katsnelson, R Yang, EW Hill, KS Novoselov, and AK Geim. Chaotic dirac billiard in graphene quantum dots. *Science*, 320(5874):356–358, 2008.
- [10] Maria AH Vozmediano, MI Katsnelson, and Francisco Guinea. Gauge fields in graphene. *Physics Reports*, 496(4-5):109–148, 2010.
- [11] Alexander Weiße, Gerhard Wellein, Andreas Alvermann, and Holger Fehske. The kernel polynomial method. *Reviews of modern physics*, 78(1):275, 2006.
- [12] Tahir Yusufaly, David Vanderbilt, and Sinisa Coh. Tight-binding formalism in the context of the pythtb package, 2013.
- [13] Yuanbo Zhang, Yan-Wen Tan, Horst L Stormer, and Philip Kim. Experimental observation of the quantum hall effect and berry’s phase in graphene. *nature*, 438(7065):201, 2005.